frontiers | Frontiers in Physiology

ORIGINAL RESEARCH
published: 04 April 2022
doi: 10.3389/fphys.2022.852946

Changes in Blood Cell Deformability in Chorea-Acanthocytosis and Effects of Treatment With Dasatinib or Lithium

*Felix Reichel[1,2], Martin Kräter[1,2], Kevin Peikert[3,4], Hannes Glaß[3], Philipp Rosendahl[2], Maik Herbig[1,2], Alejandro Rivera Prieto[2], Alexander Kihm[5], Giel Bosman[6], Lars Kaestner[5,7], Andreas Hermann[3,4,8,9] and Jochen Guck[1,2]**

[1]Max-Planck-Institut für die Physik des Lichts and Max-Planck-Zentrum für Physik und Medizin, Erlangen, Germany, [2]Biotechnology Center, Center for Molecular and Cellular Bioengineering, Technische Universität Dresden, Dresden, Germany, [3]Translational Neurodegeneration Section "Albrecht Kossel", Department of Neurology, University Medical Center Rostock, University of Rostock, Rostock, Germany, [4]Division for Neurodegenerative Diseases, Department of Neurology, Technische Universität Dresden, Dresden, Germany, [5]Department of Experimental Physics, Saarland University, Saarbrücken, Germany, [6]Department of Biochemistry, Radboud UMC, Nijmegen, Netherlands, [7]Theoretical Medicine and Biosciences, Saarland University, Homburg, Germany, [8]Deutsches Zentrum für Neurodegenerative Erkrankungen (DZNE), Rostock/Greifswald, Rostock, Germany, [9]Center for Regenerative Therapies Dresden, Technische Universität Dresden, Dresden, Germany

OPEN ACCESS

Edited by:
Aljaz Godec,
Max Planck Institute for Biophysical Chemistry, Germany

Reviewed by:
Yang Jun Kang,
Chosun University, South Korea
Asya Makhro,
University of Zurich, Switzerland

***Correspondence:**
Jochen Guck
jochen.guck@mpl.mpg.de

Specialty section:
This article was submitted to Biophysics, a section of the journal Frontiers in Physiology

Received: *11 January 2022*
Accepted: *08 March 2022*
Published: *04 April 2022*

Citation:
Reichel F, Kräter M, Peikert K, Glaß H, Rosendahl P, Herbig M, Rivera Prieto A, Kihm A, Bosman G, Kaestner L, Hermann A and Guck J (2022) Changes in Blood Cell Deformability in Chorea-Acanthocytosis and Effects of Treatment With Dasatinib or Lithium. Front. Physiol. 13:852946. doi: 10.3389/fphys.2022.852946

Misshaped red blood cells (RBCs), characterized by thorn-like protrusions known as acanthocytes, are a key diagnostic feature in Chorea-Acanthocytosis (ChAc), a rare neurodegenerative disorder. The altered RBC morphology likely influences their biomechanical properties which are crucial for the cells to pass the microvasculature. Here, we investigated blood cell deformability of five ChAc patients compared to healthy controls during up to 1-year individual off-label treatment with the tyrosine kinase inhibitor dasatinib or several weeks with lithium. Measurements with two microfluidic techniques allowed us to assess RBC deformability under different shear stresses. Furthermore, we characterized leukocyte stiffness at high shear stresses. The results showed that blood cell deformability–including both RBCs and leukocytes - in general was altered in ChAc patients compared to healthy donors. Therefore, this study shows for the first time an impairment of leukocyte properties in ChAc. During treatment with dasatinib or lithium, we observed alterations in RBC deformability and a stiffness increase for leukocytes. The hematological phenotype of ChAc patients hinted at a reorganization of the cytoskeleton in blood cells which partly explains the altered mechanical properties observed here. These findings highlight the need for a systematic assessment of the contribution of impaired blood cell mechanics to the clinical manifestation of ChAc.

Keywords: chorea-acanthocytosis, blood cell deformability, real-time deformability cytometry, dasatinib, lithium, cell mechanics

INTRODUCTION

Chorea-acanthocytosis/VPS13A disease (ChAc) is a rare monogenetic neurodegenerative disease of the young adulthood affecting multiple systems other than the central nervous system, e.g., the red blood cells (RBCs) (Jung et al., 2011; Walker, 2017; Peikert et al., 2018). ChAc is characterized by various movement disorders (due to a degeneration mainly of striatal neurons), epilepsy, cognitive decline and misshaped spiky RBCs, the latter being referred to as acanthocytes (Critchley et al., 1968;

Levine et al., 1968; Jung et al., 2011; Peikert et al., 2018). The autosomal-recessive condition is caused by loss of function mutations in the *vacuolar protein sorting 13 homolog A* (*VPS13A*) gene (Rampoldi et al., 2001; Ueno et al., 2001; Dobson-Stone et al., 2002; Danek et al., 2012; Nishida et al., 2019). Therefore, the term "VPS13A disease" has been recommended to replace the historical, more descriptive terminology (Walker and Danek, 2021). A disease-modifying therapy has not been established so far.

It is still unclear, how exactly the loss of function of VPS13A leads to the manifestation of the cellular and clinical phenotype. VPS13A localizes at different membrane contact sites and is most probably involved in non-vesicular lipid transport as it is assumed also for the other members of the VPS13 protein family (for review, see Leonzino, Reinisch and De Camilli, 2021) (Gao and Yang, 2018; Kumar et al., 2018; Yeshaw et al., 2019; Leonzino et al., 2021). Two downstream mechanisms are considered to be important drivers of ChAc pathophysiology: decreased phosphoinositide-3-kinase (PI3K) signaling and increased activity of Src family tyrosine kinase Lyn (for review, see Peikert et al., 2018 (Peikert et al., 2018)).

Active Lyn kinase accumulates in ChAc RBCs and hyperphosphorylates membrane proteins such as band 3 protein. Since band 3 is a structural protein, linking the cytoskeleton to the plasma membrane, it is likely to be causally involved in the genesis of the spiky morphology. Accumulation of active Lyn kinase was also found to be related to impaired autophagic flux (De Franceschi et al., 2011; Lupo et al., 2016). These phenotypes could be reversed by *in vitro* treatment with tyrosine kinase inhibitors (TKI) such as the Src kinase family inhibitor dasatinib (Lupo et al., 2016). In a *Vps13a* knockout mouse model, another TKI, nilotinib, improved both the hematological and neurological phenotypes by improving autophagy and preventing neuroinflammation (Peikert et al., 2021a). In their recent work, Peikert et al., 2021 (Peikert et al., 2021b) report on single individual treatment approaches targeting Lyn kinase with dasatinib in ChAc patients. They showed that initially reduced F-actin signal, increased osmotic fragility and impaired autophagy were partially restored in ChAc RBCs.

Furthermore, disturbed signaling via Phosphoinositide-3-kinase (PI3K) has been also identified as relevant in the pathophysiology of ChAc patients. Reduced signaling via the PI3K-Rac1-PAK pathway was reported to lead to disordered actin polymerization (Föller et al., 2012). Additionally, in other cells, altered PI3K signaling caused a decreased ORAI1 expression and store-operated Ca^{2+} entry (SOCE), subsequently disturbed Ca^{2+} homeostasis and apoptosis which could be partly reversed by *in vitro* lithium treatment (Yu et al., 2016; Pelzl et al., 2017a; Pelzl et al., 2017b).

The rather late onset of the disease at the age of early adulthood and the slow progression rate (Rampoldi et al., 2002; Jung et al., 2011; Walker, 2017) lead to the assumption of a dependency between the altered RBC properties and neuronal degeneration: Changes in the mechanical properties of the RBCs and hence reduced passage in micro-vessels and capillaries may impair oxygen supply in certain areas of the brain that could over time accumulate to tissue alterations leading to the symptoms described (Adjobo-Hermans et al., 2015).

Altered RBC morphology is often linked to a change in cell mechanics which may lead to impaired blood flow (An and Mohandas, 2008; Da Costa et al., 2013). Until now, the effect of acanthocytes in ChAc patients on the pathophysiology of the disease remains elusive. Here, we describe, for the first time, altered deformability of blood cells from ChAc patients including white blood cells (WBCs). In a second step, we observed these parameters during individual off-label treatments with dasatinib or lithium, each targeting one of the signaling pathways believed to be involved in the genesis of the RBC phenotype.

Deformability was measured using two techniques that asses the response to different ranges of shear stresses acting on the cells: shape analysis of RBCs at low shear stress (0.1–3 Pa) (Reichel et al., 2019) and real-time fluorescence and deformability cytometry (RT-FDC) (Otto et al., 2015; Rosendahl et al., 2018) at high shear stress (ca. 100 Pa). RBC shape analysis only assesses the deformability of RBCs because the stresses are too low to deform WBCs and the throughput is too low to measure a sufficient number of WBCs. In contrast, RT-FDC was used to characterize the mechanics of both, RBCs and WBCs. In RT-FDC on RBCs, the interpretation of the deformation data is not as straight forward as for the RBC shape analysis because the RBCs undergo a non-trivial shape change here. We chose to use both methods to have a comprehensive image of the blood cell deformability at different stresses. We demonstrate that the deformability of all blood cells is affected in ChAc patients and this is further modulated by the treatments. This highlights that monitoring blood cell mechanical properties of ChAc patients during the course of disease and possible treatments can increase our understanding of this disease.

MATERIALS AND METHODS

Cell Source and Reagents

We included five ChAc patients in this study for whom diagnosis was confirmed by Western blot (absence of chorein/VPS13A protein) and genetic testing (Dobson-Stone et al., 2004). The clinical parameters of the patients are listed in **Supplementary Table S1** and complete blood count, RBC indices and hemolytic parameters are listed in **Supplementary Table S2**. Further information for P1-P3 can be found in Peikert et al., 2021 (Peikert et al., 2021b). Patients and healthy control blood donors were enrolled in ongoing studies on the pathogenesis and natural history of neurodegenerative diseases approved by the institutional review board of the Technische Universität Dresden, Germany (EK 45022009, EK 78022015). The ChAc patients were treated with dasatinib (P1-P3) or lithium (P4-P5) in the context of an individual off-label therapy based on the above described preclinical evidence. Standard dose of 100 mg dasatinib per day was administered orally, as it was lithium for which serum lithium concentration target range was defined as 0.6–0.8 mmol/L. Treatment started after the blood for the baseline measurements was taken.

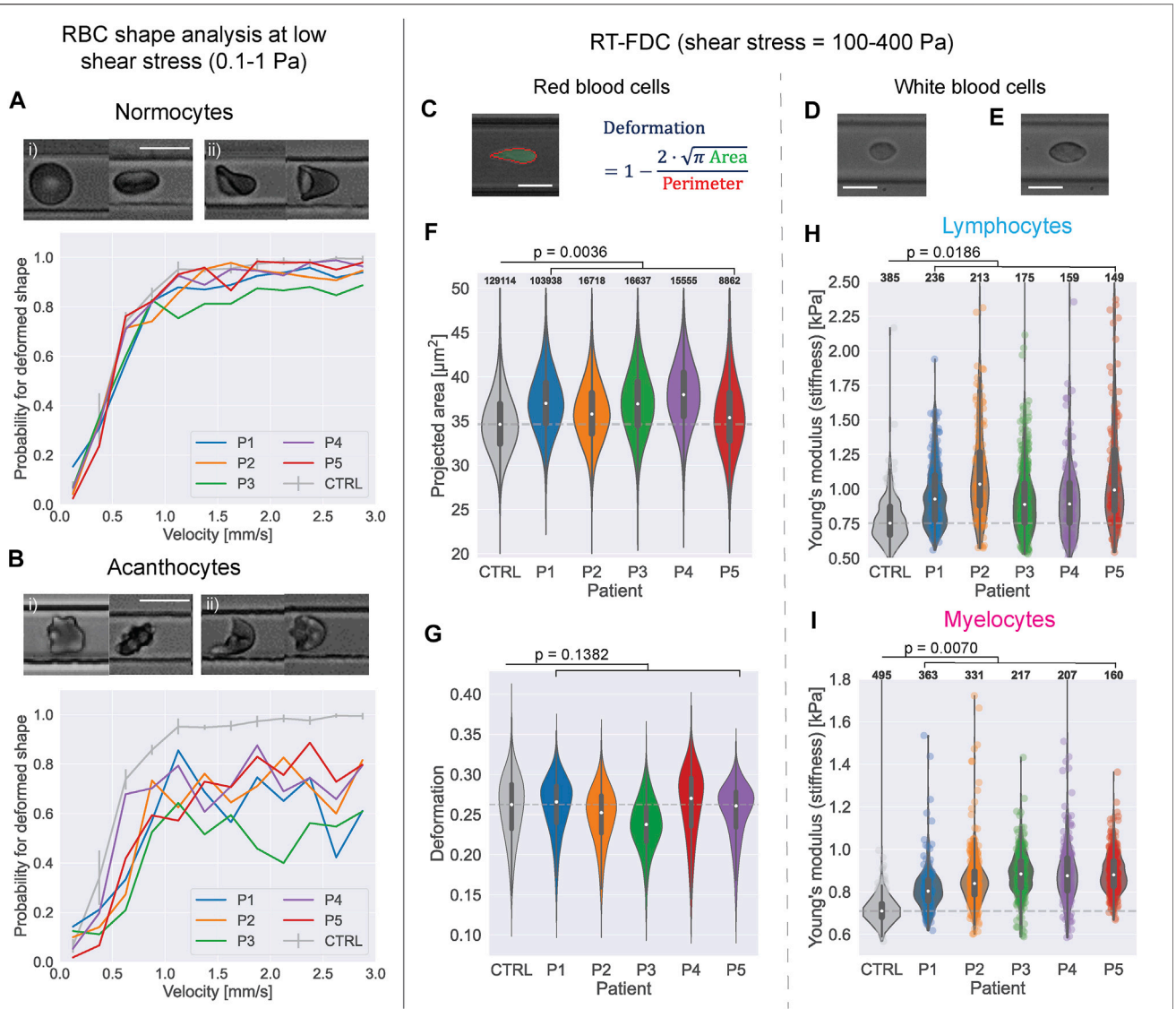

FIGURE 1 | Blood cell deformability of ChAc patients compared to healthy control blood. **(A)** Example shapes of normal, discocyte RBCs (normocytes) in an **(i)** undeformed state and **(ii)** deformed by flow during low shear stress flow in a 10 µm channel. The diagram shows the probability to find normocyte cells from the sample in a deformed state at a given cell velocity in the channel for the acanthocyte patients and the mean curve from three control measurements. Error bars represent SEM. scale bar represents 10 µm **(B)** Example shapes of acanthocytes in an **(i)** undeformed state and **(ii)** deformed by flow. Below is the shape probability diagram for the acanthocytes and the control curves. **(C)** Example shape of an RBC in RT-FDC and representation how the deformation parameter is computed. All scale bars represent 10 µm. **(D)** Example image of a lymphocyte in RT-FDC. **(E)** Example image of a myelocyte. **(F) (G)** Projected area within the contour and deformation of RBCs of the ChAc patients from RT-FDC measurements vs pooled data from 10 control measurements (full data in **Supplementary Figure S4**). White dots represent the median value; grey box in the violin shows inter-quartile range (IQR) and extended lines 1.5×IQR. Dashed grey line shows the median control value. *p*-values were calculated with linear-mixed effect models as described in Herbig et al., 2018 (Herbig et al., 2018). Numbers on top of the plots indicate the number of observations per violin. **(H)** Young's modulus of lymphocytes from ChAc patients vs control (n = 1). **(I)** Young's modulus of myelocytes from ChAc patients vs control (n = 1).

RBC Shape Analysis at Low Shear Stress

The distribution of shapes for RBCs flowing through a narrow capillary at a fixed flow condition is directly linked to the distribution of shear moduli within the population. Thus, changes in the shape distribution are directly linked to a change of cell mechanics in the sample. This approach and the experimental design are described in detail in Reichel et al., 2019 (Reichel et al., 2019). Here, cells flow through a roughly 5 mm long measurement channel that is 10 µm wide, and their shapes and dynamics are tracked at the end of the channel over a length of 435 µm. Cells were recorded with the same setup used for real-time deformability cytometry (Otto et al., 2015) using a different microfluidic chip. Examples of cells flowing through the region of interest are shown in **Figures 1A,B** and in **Supplementary Videos S1-S8**.

The shape analysis introduced in Reichel et al., 2019 (Reichel et al., 2019), comprising the RBC shapes tumblers, tank-treaders, parachutes and multilobes, cannot directly be used for samples

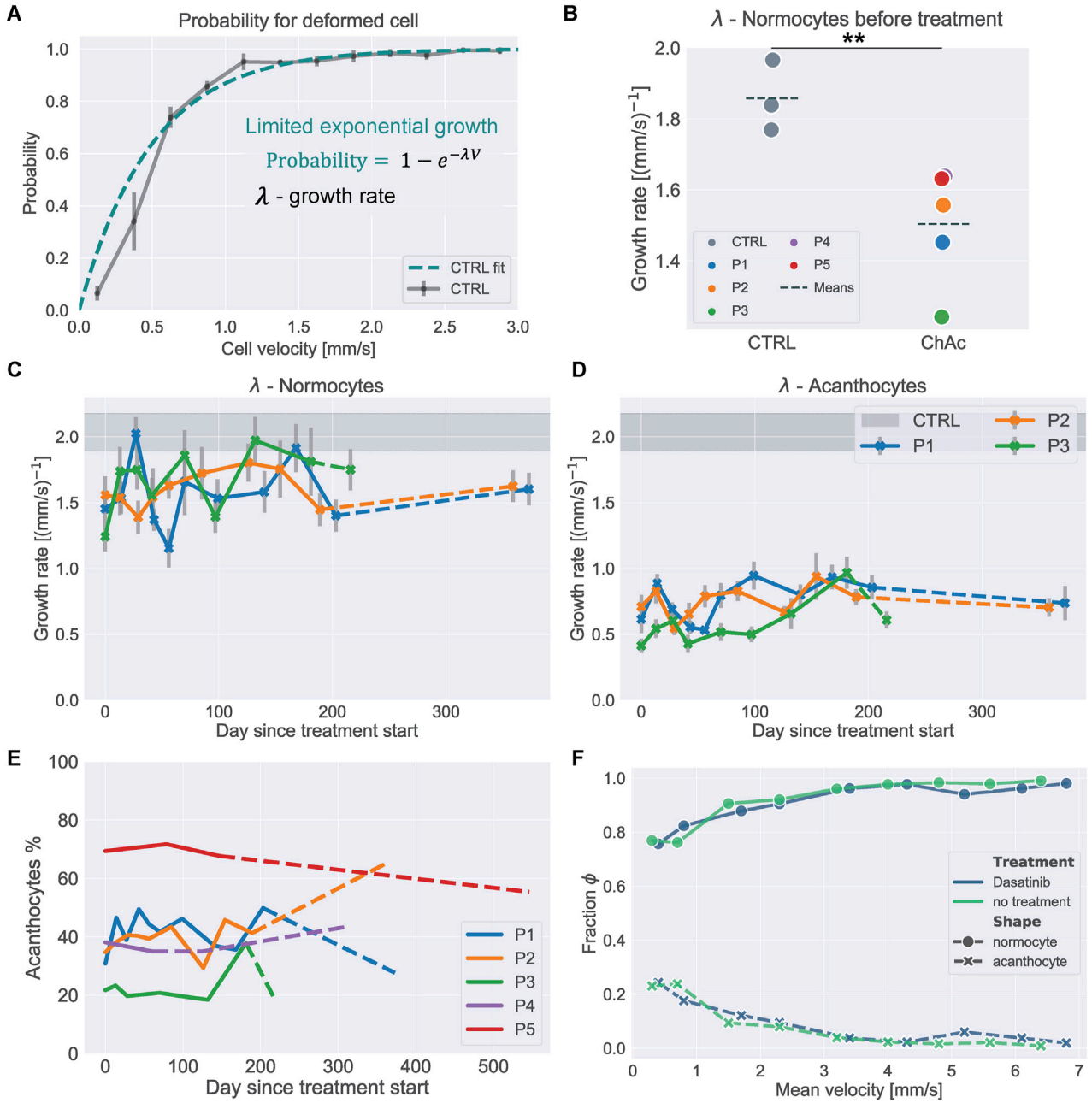

FIGURE 2 | Dasatinib treatment effect on RBC deformability. **(A)** Illustration of the limited exponential growth function fit, used to characterize the shape probability curves presented on the control data. **(B)** Fitted growth rate for normocytes of control samples vs. samples from ChAc patients. *p*-value calculated by Welch's *t*-test ($p = 0.009$). **(C)** Fitted growth rate λ of the shape probability curves from ChAc patients as a function of treatment time with dasatinib for normocytes and **(D)** acanthocytes respectively. Dashed lines represent datapoints taken after treatment was stopped. Errorbars represent standard error of the fit, calculated from the covariance matrix. Gray region shows the respective value from healthy donors without treatment (Mean ± SD). **(E)** Percentage of acanthocytes found in each sample during shape analysis measurements for patients P1-P5. Dashed lines indicate datapoints taken after the respective treatment already stopped. **(F)** Fraction of healthy shapes (hs) and acanthocytes (ac) over cell velocity for untreated and *in-vitro* dasatinib treated RBCs from patient P3.

containing acanthocytes because their shape at rest differs from that of healthy RBCs. Further, acanthocytes show shapes not observed for healthy cells (discocytes or normocytes) when deformed by the flow in the channel. For this study, cells flowing through a square channel with a width of 10 µm at cell velocities ranging up to 3 mm/s were characterized by their membrane morphology as normal looking (referred to as normocytes) or as acanthocytes if they showed thorn-like protrusions. We did not further distinguish between acanthocytes and echinocytes but argue that the mechanical

properties of both cell types should be very close (Rabe et al., 2021). Furthermore, cells were classified as either deformed by the flow or still maintaining their resting shape (undeformed). This classification was done by eye. We chose the channel dimension of 10 × 10 μm because in such channels, RBCs undergo a sharp transition from undeformed discocyte to parachute shape with a low probability of other transient shapes (Reichel et al., 2019) which makes it well suited to describe the deformed state of the cells. A change of the cell mechanical properties should manifest in a change of the fraction of deformed cells in the sample and that the velocity at which the majority of RBCs get deformed is shifted to higher values. For examples see **Figures 1A,B**.

The classification was done by eye from the recorded videos of cells passing the region of interest. This resulted in a curve with probabilities to find cells in a deformed state for a given range of velocities. The resulting curve for healthy RBCs is given in **Figure 2A** (data from Reichel et al., 2019 (Reichel et al., 2019), three control samples). To characterize differences to ChAc patient cells and changes on the cells during treatment, a limited exponential growth function $P = 1 - e^{-\lambda \cdot v}$, with cell velocity v, was fitted to the data. With this function, the probability to deform at $v = 0$ is zero and for very high velocities the probability converges to 100% which motivated this function because cells will eventually deform at high velocities. The cell deformability is characterized with the *growth rate* λ which describes how quickly the cells reach a deformed state. The fitted curve for the control values is also depicted in **Figure 2A**. A higher growth rate would indicate that cells are more deformable.

The shape analysis method is not suited to measure the deformability of WBCs, because the stresses acting the cells are too low and also the throughput of the method is not high enough to capture a sufficient number of cells.

Real-Time Fluorescence and Deformability Cytometry

The setup of real-time fluorescence and deformability cytometry (RT-FDC) is described in detail in Otto et al., 2015 (Otto et al., 2015) and Rosendahl et al., 2018 (Rosendahl et al., 2018). In brief, flow is introduced into a microfluidic chip with the help of syringe pumps and cells get deformed by hydrodynamic stresses as they pass a narrow constriction, still larger than their own size. The chip is mounted on an inverted microscope (Axiovert 200M, ZEISS, Oberkochen, Germany) and images are obtained at the end of the constriction with a CMOS camera (Mikrotron, Unterschleissheim, Germany). Camera and syringe pump are controlled via the measuring software ShapeIn (Zellmechanik Dresden, Dresden, Germany). ShapeIn analyzes the recorded images in real-time and computes a contour and projected area for each cell. The deformation parameter used in RT-FDC is defined as 1-circularity and is calculated from the contour's area and perimeter using: $\text{deformation} = 1 - 2 \cdot \sqrt{\pi \cdot \text{Area}}/\text{perimeter}$, illustrated on the example of a deformed RBC in **Figure 1C**. As introduced by Toepfner et al., 2018 (Toepfner et al., 2018), the data from RT-FDC experiments can be used to distinguish between different types of blood cells. These strategies were used here to selectively study the deformation and mechanics of RBCs, lymphocytes, and myelocytes from ChAc patients (see also SI text and **Supplementary Figure S5A,B**).

Because the stresses required to deform RBCs are smaller than for leukocytes, both were measured under different conditions. For measurements on leukocytes, citrate blood was resuspended in a viscosity-adjusted measurement buffer (phosphate saline buffer without Mg^{2+} and Ca^{2+} (PBS–) containing 0.5% (w/v) methyl cellulose (4,000 cPs, Alfa Aesar 036,718.22, CAS# 9,004–67–5); adjusted in HAAKE Falling Ball Viscometer type C (Thermo Fisher Scientific, Dreieich, Germany) using ball number three to a viscosity of 15 mPa s) at a ratio of 1:20. The increased viscosity of the buffer also increases the stresses acting on the cells inside the channel. Measurements were performed in channels with 20 × 20 μm cross-section at a flow rate of 0.08 μL/s. Example images of a deformed lymphocyte and myelocyte are shown in **Figures 1D,E**, respectively. To decouple effects of the cell size on the deformation, the Young's modulus was computed for leukocytes as described in Mokbel et al., 2017 (Mokbel et al., 2017). Since the derivation of Young's moduli for this system is only valid for initially spherical cells (Mietke et al., 2015; Mokbel et al., 2017), it cannot be calculated for RBCs.

RBC measurements were performed on an RT-FDC setup with a fluorescence module described in detail in Rosendahl et al., 2018 (Rosendahl et al., 2018). Whole blood was resuspended in the same measurement buffer described above at a ratio of 1:200. The buffer was complemented with 2.5 μM syto13 nucleic acid stain (Thermo Fisher Scientific, Dreieich, Germany) to mark for the reticulocytes in the sample. Fluorescence was excited with a 60 mW, 488 nm laser at 8% power (OBIS 488-nm LS 60 mW, Coherent Deutschland) and the signal was measured with an avalanche photodiode (MiniSM10035; SensL Corporate, Cork, Ireland). Measurements were performed in channels with a 20 × 20 μm cross-section at a flow rate of 0.02 μL/s. The control data for the RT-FDC measurements on RBCs was not measured for this study but taken from 10 control samples for Rosendahl et al., 2018 (Rosendahl et al., 2018) which were measured under the same conditions (data shown in **Supplementary Figure S4E,F**).

RESULTS

Red Blood Cell Deformability in Chorea-Acanthocytosis

To investigate differences in the deformability of red blood cells (RBCs) from chorea-acanthocytosis (ChAc) patients compared to that of healthy donors, we performed shape-analysis and real-time fluorescence and deformability cytometry (RT-FDC) measurements on the blood of five patients (P1-P5) and compared it to measurements of healthy controls. The results are depicted in **Figures 1A,B,F,G**. Every velocity bin of 0.25 mm/s in **Figures 1A,B** includes approx. 100 cells for each patient. The shape-probability curves of normocytes (**Figure 1A**) and acanthocytes (**Figure 1B**) show that RBCs from ChAc patients are less likely to deform in channel flow. It should be mentioned that also control samples can include acanthocyte-like cells but to a much lesser extent than in patient samples. The analysis for the

control samples only included normocytes. Acanthocytes are clearly less likely to deform due to flow even for higher flow velocities.

Analysis of the exponential growth rate (see **Figure 2A**) of control and ChAc normocytes is depicted in **Figure 2B** and showed that the growth rate for control normocytes was higher which indicated that the cells were more deformable. This is in line with findings from Rabe et al., 2021 (Rabe et al., 2021) which reported similar results for ChAc normocytes. A comparison for acanthocytes was not possible because they were not present in sufficient numbers in control samples.

The RT-FDC measurements showed that the RBCs of ChAc patients had a slightly larger projected area than those from healthy donors (**Figure 1F**, effect size of +1.89 μm^2, $p = 0.0036$ computed with linear mixed effect models (Herbig et al., 2018)). No significant difference between control and ChAc RBCs' deformation could be detected ($p = 0.1382$, **Figure 1G**).

White Blood Cell Deformability in Chorea-Acanthocytosis

In RT-FDC measurements on whole blood it is possible to distinguish different cell types (see materials and methods, SI text and Töpfner et al., 2018 (Toepfner et al., 2018)). Thus, we investigated mechanical differences also between the leukocytes of ChAc patients and one healthy donor. We distinguished, mainly by size, between all lymphocytes and cells resulting from the myeloid lineage without RBCs (myelocytes), comprising all mono- and granulocytes. The myelocyte fraction mainly consisted of neutrophil granulocytes (>80%).

Since white blood cells are spherical at rest, we can use a model that maps the projected area and the deformation to an apparent Young's modulus (Mokbel et al., 2017), to see differences in stiffness before, during and after the treatments. As depicted in **Figures 1H,I**, both lymphocytes and myelocytes of ChAc patients were significantly stiffer than their healthy counterparts before treatment onset (lymphocytes: +240 Pa, $p = 0.0186$, myelocytes: +150 Pa, $p = 0.0070$; effect sizes and p-values determined by linear mixed effects model analysis (Herbig et al., 2018)). The projected area and deformation data used to compute the Young's modulus is shown in **Supplementary Figure S5C,D**.

Dasatinib and Lithium Treatment Effect on RBC Deformability

RBC Shape Analysis During Dasatinib or Lithium Treatment

To study the effect of dasatinib or lithium on RBC deformability of ChAc patients, we monitored RBCs during treatment with shape analysis measurements and RT-FDC.

To compare shape-analysis data over the treatment time, a limited exponential growth was fitted to the data (see **Figure 2A**) and the fitted growth rate was used to detect changes in the deformability during the treatment time. The results for the dasatinib treatment are shown in **Figures 2C,D**, those of the lithium in **Figure 3**. Even though one might get the impression that the growth rate showed a slight increase with dasatinib treatment time for both normocytes and acanthocytes, the overall RBC deformability remained unaffected by the treatment. The results pooled for all RBCs are shown in **Supplementary Figure S1** and the curves from all measurements are given in **Supplementary Figure S2**.

The acanthocyte count over the treatment is given in **Figure 2E** and shows that the fraction of acanthocytes remained constant within a certain range of fluctuation without a systematic trend for both treatments, which was in line with the clinical data (Peikert et al., 2021b).

To check if dasatinib had a short-term effect on RBC deformability, RBCs from P3 were treated with dasatinib *in vitro* and the shapes in channel flow were analyzed (for details, see SI text). The results are shown in **Figure 2F**. There was no significant difference in the deformability between control- and dasatinib-treated RBCs. This indicated that the observed effects on cell deformability were likely caused by long-term treatment effects, e.g., acting on erythropoiesis or indirect systemic effects.

For the lithium treatment, normocyte growth rate even increased above control values during the treatment and recovered to, or below, pre-treatment levels after the treatment was discontinued. Acanthocytes showed a slight increase in growth rate during lithium treatment. This indicated that the RBCs got softer during lithium treatment but RT-FDC results showed that the cells also got larger with the treatment (see **Figure 4**) which would make the cells more likely to deform in the channel if the overall mechanics are unchanged.

RBC Deformation in RT-FDC During Dasatinib or Lithium Treatment

RT-FDC results for the dasatinib treatment are shown in **Figures 4A–C** and for the lithium treatment in **Figures 4D–F**. It can be seen that during treatment with dasatinib, the RBC deformation parameter dropped for all patients between 50–100 days after treatment start, while the projected area remained mainly constant with the exception of some outliers.

For the lithium treatment, the RT-FDC results showed that the deformation parameter decreased with treatment time which was accompanied by an increase in cell size. After the treatment, the deformation and area values returned almost to the control values for P5 while the values for P4 did not fully recover.

The interpretation of deformation values for RBCs in RT-FDC cannot directly be linked to cell mechanics because they undergo a non-trivial shape transition from discocyte to tear-drop shape (Reichel et al., 2019). A decrease of the deformation value does not necessarily mean that the cells got stiffer. To back this up, we artificially stiffened RBCs from healthy donors with glutaraldehyde (Forsyth et al., 2010; Holmes et al., 2014) or diamide (Sinha et al., 2015) (see SI text and **Supplementary Figure S3**) and saw that an increasing concentration of the reagents led to an increase of the deformation when working at low concentrations. At high concentrations the cell shape got fixed which led to lower deformation values.

Since reticulocytes have been reported to have a higher projected area and lower deformation compared to the whole RBC population (Rosendahl et al., 2018), we speculated that

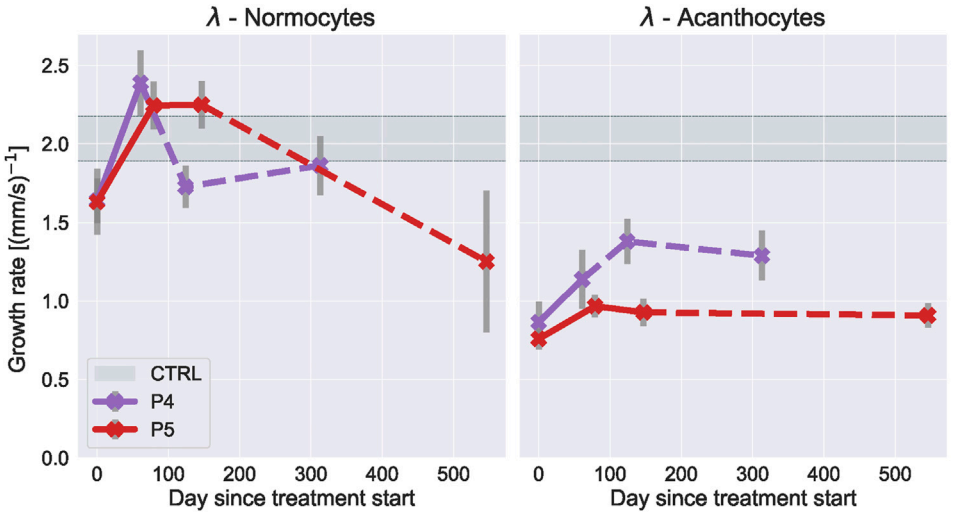

FIGURE 3 | Lithium treatment effect on RBC deformability. (one column figure) Fitted growth rate λ of the shape probability curves from ChAc patients as a function of treatment time with lithium for normocytes and acanthocytes respectively. Dashed lines represent datapoints taken after treatment was stopped. Errorbars represent standard error of the fit, calculated from the covariance matrix. Gray region shows the respective value from healthy donors without treatment (Mean ± SD).

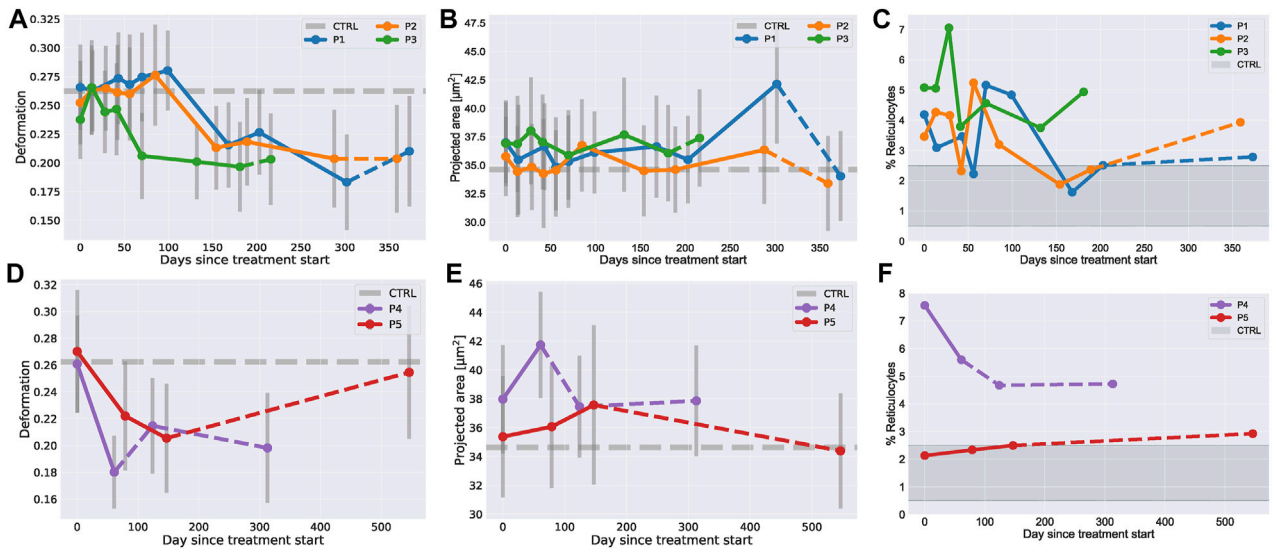

FIGURE 4 | RBC deformation, size and reticulocyte count in RT-FDC during treatment with dasatinib or lithium. **(A-C)** RBC median deformation, projected area and reticulocyte fraction measured with RT-FDC before, during and after treatment with dasatinib. **(D-F)** RBC median deformation, projected area and reticulocyte fraction measured with RT-FDC before, during and after treatment with lithium. Dashed lines indicate time points after the treatment was stopped, dashed gray lines indicate control values without treatment. The red region in the reticulocyte plots indicates the range for healthy individuals reported in the literature of 0.5–2.5%.

above mentioned results might be due to increased levels of reticulocytes in ChAc patients. The results for reticulocytes, labelled with syto13 nucleic acid stain, together with all RBCs are given in **Supplementary Figure S4A-D**. The patients' reticulocytes indeed had higher projected area and lower deformation if compared to the whole RBC population which did not differ from healthy controls. Qualitatively, reticulocyte area and deformation changed over treatment time like the total RBC population. The fraction of reticulocytes in the blood was initially higher compared to controls and slightly decreased during the dasatinib treatment closer to values from healthy donors (**Figure 4C**). A reduction of the reticulocyte count with dasatinib treatment was also reported for *VPS13a*$^{-/-}$ mice phenocopying human ChAc (Peikert et al., 2021a). During lithium treatment P4 showed a decrease during and after treatment, while P5 showed a slight increase but values were mostly in the range expected for healthy individuals (0.5–2.5%).

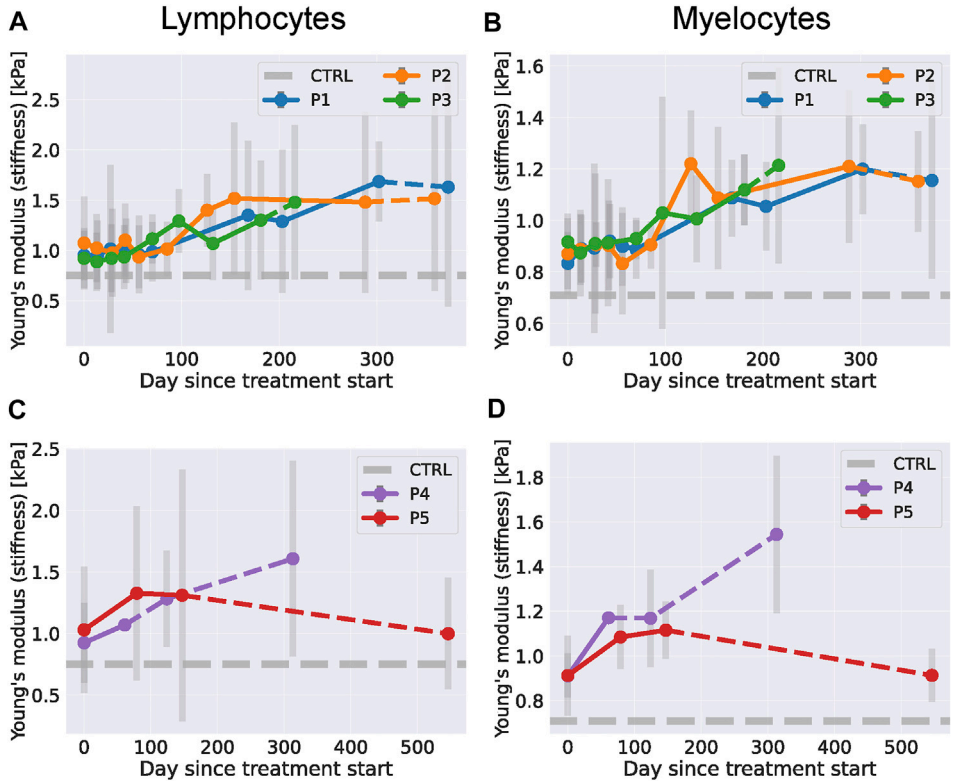

FIGURE 5 | Leukocyte stiffness in RT-FDC during treatment with dasatinib or lithium. (one column figure) **(A)** Median Young's modulus of ChAc patients' lymphocytes during dasatinib treatment. **(B)** Median Young's modulus of ChAc patients' myelocytes during dasatinib treatment. **(C)** Median Young's modulus of ChAc patients' lymphocytes during lithium treatment. **(D)** Median Young's modulus of ChAc patients' myelocytes during lithium treatment.

ChAc Leukocytes Stiffened During Treatment With Dasatinib

The Young's moduli of lymphocytes and myelocytes in dasatinib treatment are shown in **Figures 5A,B**. The lithium data is shown in **Figures 5C,D**. During treatment with dasatinib, we observed a further increase of the Young's modulus for all three patients which also persisted for the lymphocytes shortly after the treatment stopped. For myelocytes, the median Young's modulus decreased for patients P1 and P2 shortly after the treatment but kept increasing for P3.

During treatment with lithium both patients showed an increase in lymphocyte and myelocyte stiffness. After the treatment was stopped, we observed a further increase for patient P4 and a drop back to the pre-treatment level for patient P5 approximately 1 year after the treatment stopped. The area and deformation data used to compute the Young's modulus is given in **Supplementary Figure S5E,F**.

DISCUSSION

Our study highlights that the deformability, not only of RBCs but of all blood cell types, was altered in ChAc patients. Shape analysis results showed a decreased deformability of ChAc RBCs compared to controls. The decreased deformability can be directly inferred from the reduced number of deformed cells at any cell velocity which was also reflected by a smaller growth rate. A reduced deformability of ChAc normocytes, deduced from cell shapes, has recently also been reported by Rabe et al., 2021 (Rabe et al., 2021).

In RT-FDC, we did not observe a change in the deformation parameter but ChAc RBCs had a larger projected area. Because deformation and size are always correlated in RT-FDC (Mietke et al., 2015), this is also an indicator for a change of RBC deformability, but the interpretation of this behavior is not straight forward. To see how the deformation parameter changes when RBC stiffness is controllably changed, we treated RBCs *in vitro* with glutaraldehyde or diamide. At low concentrations, we observed an increase of the deformation parameter which shows that higher deformation parameter can also occur for stiffer RBCs.

While we observed larger RBCs in ChAc patients, values for the mean corpuscular volume (MCV) reported in Peikert et al., 2021 (Peikert et al., 2021b) (see also **Supplementary Table S2**) did not show an increased RBC volume for patients P1-P3. Sizes reported in RT-FDC measurements are based on the projected cross-sectional area of the deformed cells. Simulations of the flow fields inside the channel suggest that the stresses near the centerline can be approximated as axisymmetric (Panhwar et al., 2020). Therefore, it is fair to assume that the RBCs take up an axisymmetric shape as

well and the projected area is directly correlated to cell size. In automated cell counters, the MCV is determined, e.g., by impedance or light scattering measurements which require a constant deformability of RBCs for a reliable result. Thus, MCV is not a direct measurement of single cell sizes. Here, we provide a direct observation of sizes based on single cell imaging.

Both, shape analysis and RT-FDC indicated a change of RBC deformability during treatment with dasatinib. Shape analysis experiments showed a slight increase of the growth rate with treatment time, which indicated an increased deformability of both normocytes and acanthocytes. In RT-FDC, we observed a sharp drop of the deformation parameter after 50–100 treatment days while the size fluctuated around a constant value. Again, for RBCs a direct link between the deformation parameter in RT-FDC and cell mechanics is not trivial and a decrease in deformation does not necessarily mean that the cells got stiffer (see **Supplementary Figure S3**). Even though we do not have certainty of the direction of the change, we claim that RBC mechanics was altered during dasatinib treatment.

During lithium treatment, we also observed an increasing growth rate in the shape analysis which indicated increased RBC deformability. In RT-FDC, we saw a decrease of deformation accompanied by an increase in projected area. An increase in projected area and decrease in deformation hints at a volume increase and a reduced surface area-to-volume ratio, which leads to an increased sphericity or effective rounding of the cells. Rounder shapes lead to smaller deformation values, assuming that this effect dominates any stiffness changes of the cells. The increased cell size could also explain the increased deformability in the shape analysis experiments because larger cells experience higher stresses and are therefore more likely to deform. All in all, these findings indicate that lithium affects RBC properties in ChAc patients but because of the scarcity of the data here, one should be careful with the interpretation.

Data from Peikert et al., 2021 indicated that with dasatinib treatment, F-actin became more localized at the cortex (Peikert et al., 2021b). These modifications in the actin network likely contribute to changes in RBC deformability (Gokhin et al., 2015) that we observed here.

Treatment with dasatinib led to a decrease of the reticulocyte fraction in the blood of ChAc patients. The same effect was observed in a mouse model phenocopying human ChAc (Peikert et al., 2021a). Peikert et al., 2021 reported an abundance of the autophagy initiator Ulk1 in ChAc patients RBCs, which decreased with dasatinib treatment (Peikert et al., 2021b). Ulk1 is connected to autophagy in erythropoiesis and could influence the rate of reticulocyte production (Kundu et al., 2008), providing a mechanistic link to the reticulocyte count.

While an impaired RBC deformability was described before for patients with other forms of neuroacanthocytosis (Cluitmans et al., 2015) this is, to our knowledge, the first time that also patients' leukocyte stiffness was studied. Lymphocytes and myelocytes were both stiffer in ChAc patients compared to cells from healthy donors. This is of interest as *VPS13A*, the gene which is known to have a loss-of-function mutation in ChAc, is especially expressed in human monocytes and B-, and helper T-cells (Samaras et al., 2019). Since VPS13A is known to cause structural reorganizations of the cytoskeleton from studies on other cell types (De Franceschi et al., 2011; Föller et al., 2012; Rzepnikowska et al., 2017), it is likely that we observed these as altered mechanical properties in leukocytes. Another feature in ChAc blood is an increased expression of Lyn kinase, which is known to set the threshold for B-cell activation. Mechanical changes of lymphocytes after activation have been reported before (Toepfner et al., 2018; Zhang et al., 2020). Another mechanism that could lead to altered leukocyte mechanics is an increase in interleukin-1 beta (IL-1b) that was observed in the brain of *Vps13a* knockout mice (Peikert et al., 2021a). IL-1b not only plays a key role in autoinflammation but is also known to cause re-organization of the actin cytoskeleton in different cell types (Franco-Barraza et al., 2010; Lie et al., 2012).

Young's moduli of both lymphocytes and myelocytes increased even further away from control values during treatment with dasatinib or lithium. A stiffening was previously also observed for leukemic cells during treatment with different chemotherapeutic agents for acute lymphoblastic leukemia (dexamethasone and daunorubicin), such as dasatinib (Lam et al., 2007). Dasatinib interferes with all the pathways described above and likely induces further mechanical changes in leukocytes. The inhibited activity of Lyn during dasatinib treatment could cause a change in lymphocyte activation levels leading to altered mechanics but the exact mechanisms for the observed leukocyte stiffening with dasatinib treatment remain rather speculative at this point.

Overall, our results showed that the mechanical phenotype of all blood cell types in ChAc patients were impaired but did not change towards regimes of healthy donors during the treatments. Clinical data in Peikert et al., 2021 (Peikert et al., 2021b) hints on slightly improved hematological features but these did not manifest in an improved neurological phenotype. This demonstrates that the techniques that were utilized here are suited to measure a treatment response.

In general, decreased blood cell deformability often leads to clinical symptoms due to decreased cell survival and secondary pathology (Brown et al., 2005; An and Mohandas, 2008; Da Costa et al., 2013; Adjobo-Hermans et al., 2015). Especially, an impaired oxygen transport by altered blood cell deformability should be considered in neurological diseases (Kikuchi et al., 1994). While clinical descriptions of ChAc patients focus on neurological symptoms, we highlight in this study that the effects on blood deformability should not be neglected and could contribute to the clinical manifestation (through the mechanisms stated above) and thus methods that are able to monitor this (as shown here) should be considered as read outs for clinical trials. Our results on the impaired mechanics of leucocytes especially highlights that the focus of ChAc research should not only be on RBCs but also include other blood cell types.

DATA AVAILABILITY STATEMENT

Data was analyzed and plotted using custom python scripts. A detailed documentation can be found here: https://gitlab.gwdg.de/freiche/changes-in-blood-cell-deformability-in-chorea-acanthocytosis-and-effects-of-treatment-with-dasatinib-or-lithium. A collection of the raw data files is on figshare: https://doi.org/10.6084/m9.fshare.c.5793482.

ETHICS STATEMENT

The studies involving human participants were reviewed and approved by Institutional review board of the Technische Universität Dresden, Germany (EK 45022009, EK 78022015). The patients/participants provided their written informed consent to participate in this study.

AUTHOR CONTRIBUTIONS

Conceptualization: FR, MK, KP, GB, AH, and JG; Experiments–shape analysis: FR and ARP., Experiments–RT-FDC: FR, PR, MH, and MK, Experiments–in-vitro shape analysis: AK; Formal analysis: FR, PR, AK, and MK; Supervision: LK, AH, and JG; Writing–original draft, KP and FR; Writing–review and editing, FR, MK, KP, GB, LK, AH, and JG; All authors have read and agreed to the published version of the manuscript.

FUNDING

KP was supported by the Else Kröner Forschungskolleg Dresden and the MeDDrive program (TU Dresden, Germany), as well as by the Rostock Academy for Clinician Scientists (RACS) and the FORUN program (University of Rostock, Germany). AH was supported by the "Hermann und Lilly Schilling-Stiftung für medizinische Forschung im Stifterverband". Expenses for the off-label dasatinib prescription were gratefully covered in part by the Center for Regenerative Therapies Dresden (CRTD, TU Dresden, Germany) and the public healthcare insurance of the patients.

ACKNOWLEDGMENTS

The authors thank all patients and their families for giving consent for publication of the data and the healthy control subjects for participation in this study. We are especially grateful to Glenn (†) and Ginger Irvine as the founders of the Advocacy for Neuroacanthocytosis Patients (www.naadvocacy.org) and to Susan Wagner and Joy Willard-Williford as representatives of the NA Advocacy United States (www.naadvocacyusa.org).

SUPPLEMENTARY MATERIAL

The Supplementary Material for this article can be found online at: https://www.frontiersin.org/articles/10.3389/fphys.2022.852946/full#supplementary-material

REFERENCES

Adjobo-Hermans, M. J. W., Cluitmans, J. C. A., and Bosman, G. J. C. G. M. (2015). Neuroacanthocytosis: Observations, Theories and Perspectives on the Origin and Significance of Acanthocytes. *Tremor and Other Hyperkinetic Movements* 5, 328. doi:10.5334/tohm.271

An, X., and Mohandas, N. (2008). Disorders of Red Cell Membrane. *Br. J. Haematol.* 141, 367–375. doi:10.1111/j.1365-2141.2008.07091.x

Brown, C. D., Ghali, H. S., Zhao, Z., Thomas, L. L., and Friedman, E. A. (2005). Association of Reduced Red Blood Cell Deformability and Diabetic Nephropathy. *Kidney Int.* 67 (1), 295–300. doi:10.1111/j.1523-1755.2005.00082.x

Cluitmans, J. C. A., Tomelleri, C., Yapici, Z., Dinkla, S., Bovee-Geurts, P., Chokkalingam, V., et al. (2015). "Abnormal Red Cell Structure and Function in Neuroacanthocytosis," *PLoS One*. Editor P Connes, 10, e0125580. doi:10.1371/journal.pone.0125580

Critchley, E. M. R., Clark, D. B., and Wikler, A. (1968). Acanthocytosis without. *Arch. Neurol.* 18 (2), 134–140. doi:10.1001/archneur.1968.00470320036004

Da Costa, L., Galimand, J., Fenneteau, O., and Mohandas, N. (2013). Hereditary Spherocytosis, Elliptocytosis, and Other Red Cell Membrane Disorders. *Blood Rev.* 27 (4), 167–178. doi:10.1016/j.blre.2013.04.003

Danek, A., Bader, B., Velayos-Baeza, A., and Walker, R. H. (2012). Autosomal Recessive Transmission of Chorea-Acanthocytosis Confirmed. *Acta Neuropathol.* 123 (6), 905–906. doi:10.1007/s00401-012-0971-y

De Franceschi, L., Tomelleri, C., Matte, A., Brunati, A. M., Bovee-Geurts, P. H., Bertoldi, M., et al. (2011). Erythrocyte Membrane Changes of Chorea-Acanthocytosis Are the Result of Altered Lyn Kinase Activity. *Blood* 118 (20), 5652–5663. doi:10.1182/blood-2011-05-355339

Dobson-Stone, C., Velayos-Baeza, A., Filippone, L. A., Westbury, S., Storch, A., Erdmann, T., et al. (2004). Chorein Detection for the Diagnosis of Chorea-Acanthocytosis. *Ann. Neurol.* 56 (2), 299–302. doi:10.1002/ana.20200

Dobson-Stone, C., Danek, A., Rampoldi, L., Hardie, R., Chalmers, R., and Wood, N. (2002). Mutational Spectrum of the CHAC Gene in Patients with Chorea-Acanthocytosis. *Eur. J. Hum. Genet.* 10 (11), 773–781. doi:10.1038/sj.ejhg.5200866

Föller, M., Hermann, A., Gu, S., Alesutan, I., Qadri, S. M., Borst, O., et al. (2012). Chorein–sensitive Polymerization of Cortical Actin and Suicidal Cell Death in Chorea–Acanthocytosis. *FASEB J.* 26 (4), 1526–1534. doi:10.1096/fj.11-198317

Forsyth, A. M., Wan, J., Ristenpart, W. D., and Stone, H. A. (2010). The Dynamic Behavior of Chemically "Stiffened" Red Blood Cells in Microchannel Flows. *Microvasc. Res.* 80 (1), 37–43. doi:10.1016/j.mvr.2010.03.008

Franco-Barraza, J., Valdivia-Silva, J. E., Zamudio-Meza, H., Castillo, A., García-Zepeda, E. A., Benítez-Bribiesca, L., et al. (2010). Actin Cytoskeleton Participation in the Onset of IL-1β Induction of an Invasive Mesenchymal-like Phenotype in Epithelial MCF-7 Cells. *Arch. Med. Res.* 41 (3), 170–181. doi:10.1016/j.arcmed.2010.04.010

Gao, M., and Yang, H. (2018). VPS13: A Lipid Transfer Protein Making Contacts at Multiple Cellular Locations. *J. Cel Biol* 217 (10), 3322–3324. doi:10.1083/jcb.201808151

Gokhin, D. S., Nowak, R. B., Khoory, J. A., De la Piedra, A., Ghiran, I. C., and Fowler, V. M. (2015). Dynamic Actin Filaments Control the Mechanical Behavior of the Human Red Blood Cell Membrane. Pollard TD. *Mol. Biol. Cel*. Editors T. D. Pollard. 26 (9), 1699–1710. doi:10.1091/mbc.E14-12-1583

Herbig, M., Mietke, A., Müller, P., and Otto, O. (2018). Statistics for Real-Time Deformability Cytometry: Clustering, Dimensionality Reduction, and Significance Testing. *Biomicrofluidics* 12 (4), 042214. doi:10.1063/1.5027197

Holmes, D., Whyte, G., Bailey, J., Vergara-Irigaray, N., Ekpenyong, A., Guck, J., et al. (2014). Separation of Blood Cells with Differing Deformability Using Deterministic Lateral Displacement. *Interf. Focus* 4 (6), 20140011. doi:10.1098/rsfs.2014.0011

Jung, H. H., Danek, A., and Walker, R. H. (2011). Neuroacanthocytosis Syndromes. *Orphanet J. Rare Dis.* 6 (1), 68. doi:10.1186/1750-1172-6-68

Kikuchi, Y., Da, Q-W., and Fujino, T. (1994). Variation in Red Blood Cell Deformability and Possible Consequences for Oxygen Transport to Tissue. *Microvasc. Res.* 47 (2), 222–231. doi:10.1006/mvre.1994.1017

Kumar, N., Leonzino, M., Hancock-Cerutti, W., Horenkamp, F. A., Li, P., Lees, J. A., et al. (2018). VPS13A and VPS13C Are Lipid Transport Proteins Differentially Localized at ER Contact Sites. *J. Cel Biol* 217 (10), 3625–3639. doi:10.1083/jcb.201807019

Kundu, M., Lindsten, T., Yang, C-Y., Wu, J., Zhao, F., Zhang, J., et al. (2008). Ulk1 Plays a Critical Role in the Autophagic Clearance of Mitochondria and

Ribosomes during Reticulocyte Maturation. *Blood* 112 (4), 1493–1502. doi:10.1182/blood-2008-02-137398

Lam, W. A., Rosenbluth, M. J., and Fletcher, D. A. (2007). Chemotherapy Exposure Increases Leukemia Cell Stiffness. *Blood* 109 (8), 3505–3508. doi:10.1182/blood-2006-08-043570

Leonzino, M., Reinisch, K. M., and De Camilli, P. (2021). Insights into VPS13 Properties and Function Reveal a New Mechanism of Eukaryotic Lipid Transport. *Biochim. Biophys. Acta - Mol. Cel Biol Lipids* 1866 (10), 159003. doi:10.1016/j.bbalip.2021.159003

Levine, I. M., Estes, J. W., and Looney, J. M. (1968). Hereditary Neurological Disease with Acanthocytosis. *Arch. Neurol.* 19 (4), 403–409. doi:10.1001/archneur.1968.00480040069007

Lie, P. P. Y., Cheng, C. Y., and Mruk, D. D. (2012). The Biology of Interleukin-1: Emerging Concepts in the Regulation of the Actin Cytoskeleton and Cell junction Dynamics. *Cell Mol Life Sci* 69 (4), 487–500. doi:10.1007/s00018-011-0760-0

Lupo, F., Tibaldi, E., Matte, A., Sharma, A. K., Brunati, A. M., Alper, S. L., et al. (2016). A New Molecular Link between Defective Autophagy and Erythroid Abnormalities in Chorea-Acanthocytosis. *Blood* 128 (25), 2976–2987. doi:10.1182/blood-2016-07-727321

Mietke, A., Otto, O., Girardo, S., Rosendahl, P., Taubenberger, A., Golfier, S., et al. (2015). Extracting Cell Stiffness from Real-Time Deformability Cytometry: Theory and Experiment. *Biophys. J.* 109 (10), 2023–2036. doi:10.1016/j.bpj.2015.09.006

Mokbel, M., Mokbel, D., Mietke, A., Träber, N., Girardo, S., Otto, O., et al. (2017). Numerical Simulation of Real-Time Deformability Cytometry to Extract Cell Mechanical Properties. *ACS Biomater. Sci. Eng.* 3 (11), 2962–2973. doi:10.1021/acsbiomaterials.6b00558

Nishida, Y., Nakamura, M., Urata, Y., Kasamo, K., Hiwatashi, H., Yokoyama, I., et al. (2019). Novel Pathogenic VPS13A Gene Mutations in Japanese Patients with Chorea-Acanthocytosis. *Neurol. Genet.* 5 (3), e332. doi:10.1212/NXG.0000000000000332

Otto, O., Rosendahl, P., Mietke, A., Golfier, S., Herold, C., Klaue, D., et al. (2015). Real-time Deformability Cytometry: On-The-Fly Cell Mechanical Phenotyping. *Nat. Methods* 12 (3), 199–202. doi:10.1038/nmeth.3281

Panhwar, M. H., Czerwinski, F., Dabbiru, V. A. S., Komaragiri, Y., Fregin, B., Biedenweg, D., et al. (2020). High-throughput Cell and Spheroid Mechanics in Virtual Fluidic Channels. *Nat. Commun.* 11 (1), 2190. doi:10.1038/s41467-020-15813-9

Peikert, K., Federti, E., Matte, A., Constantin, G., Pietronigro, E. C., Fabene, P. F., et al. (2021). Therapeutic Targeting of Lyn Kinase to Treat Chorea-Acanthocytosis. *Acta Neuropathol. Commun.* 9 (1), 81. doi:10.1186/s40478-021-01181-y

Peikert, K., Glaß, H., Federti, E., Matte, A., Pelzl, L., Akgün, K., et al. (2021). Targeting Lyn Kinase in Chorea-Acanthocytosis: A Translational Treatment Approach in a Rare Disease. *J. Pers Med.* 11 (5), 392. doi:10.3390/jpm11050392

Peikert, K., Danek, A., and Hermann, A. (2018). Current State of Knowledge in Chorea-Acanthocytosis as Core Neuroacanthocytosis Syndrome. *Eur. J. Med. Genet.* 61 (11), 699–705. doi:10.1016/j.ejmg.2017.12.007

Pelzl, L., Elsir, B., Sahu, I., Bissinger, R., Singh, Y., Sukkar, B., et al. (2017). Lithium Sensitivity of Store Operated Ca2+ Entry and Survival of Fibroblasts Isolated from Chorea-Acanthocytosis Patients. *Cell Physiol Biochem* 42 (5), 2066–2077. doi:10.1159/000479901

Pelzl, L., Hauser, S., Elsir, B., Sukkar, B., Sahu, I., Singh, Y., et al. (2017). Lithium Sensitive ORAI1 Expression, Store Operated Ca2+ Entry and Suicidal Death of Neurons in Chorea-Acanthocytosis. *Sci. Rep.* 7 (1), 6457. doi:10.1038/s41598-017-06451-1

Rabe, A., Kihm, A., Darras, A., Peikert, K., Simionato, G., Dasanna, A. K., et al. (2021). The Erythrocyte Sedimentation Rate and its Relation to Cell Shape and Rigidity of Red Blood Cells from Chorea-Acanthocytosis Patients in an Off-Label Treatment with Dasatinib. *Biomolecules* 11 (5), 727. doi:10.3390/biom11050727

Rampoldi, L., Danek, A., and Monaco, A. P. (2002). Clinical Features and Molecular Bases of Neuroacanthocytosis. *J. Mol. Med.* 80 (8), 475–491. doi:10.1007/s00109-002-0349-z

Rampoldi, L., Dobson-Stone, C., Rubio, J. P., Danek, A., Chalmers, R. M., Wood, N. W., et al. (2001). A Conserved Sorting-Associated Protein Is Mutant in Chorea-Acanthocytosis. *Nat. Genet.* 28 (2), 119–120. doi:10.1038/88821

Reichel, F., Mauer, J., Nawaz, A. A., Gompper, G., Guck, J., and Fedosov, D. A. (2019). High-Throughput Microfluidic Characterization of Erythrocyte Shapes and Mechanical Variability. *Biophys. J.* 117 (1), 14–24. doi:10.1016/j.bpj.2019.05.022

Rosendahl, P., Plak, K., Jacobi, A., Kraeter, M., Toepfner, N., Otto, O., et al. (2018). Real-time Fluorescence and Deformability Cytometry. *Nat. Methods* 15 (5), 355–358. doi:10.1038/nmeth.4639

Rzepnikowska, W., Flis, K., Muñoz-Braceras, S., Menezes, R., Escalante, R., and Zoladek, T. (2017). Yeast and Other Lower Eukaryotic Organisms for Studies of Vps13 Proteins in Health and Disease. *Traffic* 18 (11), 711–719. doi:10.1111/tra.12523

Samaras, P., Schmidt, T., Frejno, M., Gessulat, S., Reinecke, M., Jarzab, A., et al. (2019). ProteomicsDB: a Multi-Omics and Multi-Organism Resource for Life Science Research. *Nucleic Acids Res.* 48 (D1), D1153–D1163. doi:10.1093/nar/gkz974

Sinha, A., Chu, T. T. T., Dao, M., and Chandramohanadas, R. (2015). Single-cell Evaluation of Red Blood Cell Bio-Mechanical and Nano-Structural Alterations upon Chemically Induced Oxidative Stress. *Sci. Rep.* 5 (1), 9768. doi:10.1038/srep09768

Toepfner, N., Herold, C., Otto, O., Rosendahl, P., Jacobi, A., Kräter, M., et al. (2018). Detection of Human Disease Conditions by Single-Cell Morpho-Rheological Phenotyping of Blood. *Elife* 7, e29213. doi:10.7554/eLife.29213

Ueno, S., Maruki, Y., Nakamura, M., Tomemori, Y., Kamae, K., Tanabe, H., et al. (2001). The Gene Encoding a Newly Discovered Protein, Chorein, Is Mutated in Chorea-Acanthocytosis. *Nat. Genet.* 28 (2), 121–122. doi:10.1038/88825

Walker, R. H., and Danek, A. (2021). Neuroacanthocytosis" – Overdue for a Taxonomic Update. *Tremor and Other Hyperkinetic Movements* 11 (1), 1–6. doi:10.5334/tohm.583

Walker, R. H. (2017). "Chorea-Acanthocytosis☆," in *Reference Module in Neuroscience and Biobehavioral Psychology* Amsterdam, Netherlands: Elsevier, 217–219. doi:10.1016/B978-0-12-809324-5.00521-6

Yeshaw, W. M., van der Zwaag, M., Pinto, F., Lahaye, L. L., Faber, A. I. E., Gómez-Sánchez, R., et al. (2019). Human VPS13A Is Associated with Multiple Organelles and Influences Mitochondrial Morphology and Lipid Droplet Motility. *Elife* 8, e43561. doi:10.7554/eLife.43561

Yu, W., Honisch, S., Schmidt, S., Yan, J., Schmid, E., Alkahtani, S., et al. (2016). Chorein Sensitive Orai1 Expression and Store Operated Ca2+ Entry in Rhabdomyosarcoma Cells. *Cel Physiol Biochem* 40 (5), 1141–1152. doi:10.1159/000453168

Zhang, X., Kim, T-H., Thauland, T. J., Li, H., Majedi, F. S., Ly, C., et al. (2020). Unraveling the Mechanobiology of Immune Cells. *Curr. Opin. Biotechnol.* 66, 236–245. doi:10.1016/j.copbio.2020.09.004

Conflict of Interest: The authors declare that the research was conducted in the absence of any commercial or financial relationships that could be construed as a potential conflict of interest.

Publisher's Note: All claims expressed in this article are solely those of the authors and do not necessarily represent those of their affiliated organizations, or those of the publisher, the editors, and the reviewers. Any product that may be evaluated in this article, or claim that may be made by its manufacturer, is not guaranteed or endorsed by the publisher.